

This paper has been submitted for presentation at *American Control Conference 2025*.

This is the author's version of an article that has, or will be, published in this journal or conference.
Changes were, or will be, made to this version by the publisher prior to publication.

arXiv:2502.00215v1 [eess.SY] 31 Jan 2025

©2024 IEEE. Personal use of this material is permitted. Permission from IEEE must be obtained for all other uses, in any current or future media, including reprinting/republishing this material for advertising or promotional purposes, creating new collective works, for resale or redistribution to servers or lists, or reuse of any copyrighted component of this work in other works.

Impulsive Relative Motion Control with Continuous-Time Constraint Satisfaction for Cislunar Space Missions

Fabio Spada¹, Purnanand Elango², Behçet Açıkmeşe³

Abstract—Recent investments in cislunar applications open new frontiers for space missions within highly nonlinear dynamical regimes. In this paper, we propose a method based on Sequential Convex Programming (SCP) to loiter around a given target with impulsive actuation while satisfying path constraints continuously over the finite time-horizon, i.e., independently of the number of nodes in which domain is discretized. Location, timing, magnitude, and direction of a fixed number of impulses are optimized in a model predictive framework, exploiting the exact nonlinear dynamics of non-stationary orbital regimes. The proposed approach is validated on a relative orbiting problem with respect to a selenocentric Near Rectilinear Halo Orbit.

I. INTRODUCTION

This paper describes and tests an optimal model predictive strategy to compute constrained relative trajectories between a chaser and a target spacecraft in nonlinear time-dependent dynamical environments, with impulsive controls. We propose to use a nonlinear model of the dynamics for the relative motion. The time-invariant Clohessy-Wiltshire model works well for eccentric orbits only when their eccentricity is low [1] and is not accurate enough when strong non-Keplerian disturbances are present [2]. In multi-body scenarios, two-body models produce significant errors for propagation times similar to operational durations [3]. In all cases, the higher the distance between the chaser and the target, the less accurate the linearized model becomes, which motivates the use of the nonlinear relative dynamics model.

For safety, chaser’s motion relative to the target must satisfy certain constraints during operations. These include, for example, keep-out zones (KOZ) [4] and approach corridors (AC) [5]. Similarly, during inspection tasks, the chaser needs to stay within a keep-in zone (KIZ) close to the target [6].

A simple KIZ constraint is satisfied when the chaser passively orbits its target while keeping a finite distance from it; these orbits are known as *bounded relative orbits* (BROs). Initial conditions for BROs under zonal perturbations and for arbitrary eccentricities can be computed with both analytical [7] and numerical methods [8], [9]. *Natural loitering* can also satisfy coarse KIZ requirements. Studies on long-term loitering show its feasibility in the Earth-Moon gravity field, but confirm that the minimum and maximum distances from the target can not be chosen independently [10]. Strict KIZ

requirements need control. In *forced loitering*, shooting is used to calculate the impulsive controls that, when applied at specific waypoints, enable periodic motion through these waypoints [11], [12]; however, KIZ constraints can not be applied to the coast arcs, so their satisfaction is guaranteed only at waypoints. Chaser can stay around a specific point near the target by *hovering*. Analytical methods have been used, with simplified dynamical models, for asteroid exploration missions [13]. Numerical schemes can reduce fuel consumption or include operational constraints: impulsive control saturation [14] and finite number of impulses [15] can be integrated into a model predictive control (MPC) framework.

KOZ constraints are essential for safety, thus ensuring their satisfaction is crucial for successful missions. This aspect is taken into account both in mission planning and in control [16]. Past analyses have addressed trajectory planning with polytopic KOZ as a Mixed-Integer Linear Programming problem [17] or have included multiple KOZs in J_2 -perturbed gravitational model [18]. Robust nonlinear controllers combined with accurate KOZ models have been proposed for aggressive relative maneuvers [19]. MP formulations have been extensively tested and analyzed for close-proximity operations. Treating optimal trajectory planning as a Quadratic Program with linear constraints has proven versatile for various maneuvers [20]. Different approaches to managing nonconvex KOZ constraints have also been examined from a recursive feasibility perspective [21]. Recently, a probability-based formulation has been proposed to ensure robust satisfaction of the line-of-sight (LOS) state constraint [22]. MPC can also be combined with backward reachable sets to compute trajectories that satisfy safety constraints, even with modeled failure modes [23].

In this work, the constrained relative orbiting problem (CROP) with impulsive controls is assessed using a model predictive approach. The problem is formulated as an Optimal Control Problem (OCP) with free impulse timings. With generalized time-dilation (GTD), the control vector is augmented with the dilation factor, a positive definite scalar control [24], and physical time can be treated as an additional state. The problem is hence reformulated in the dilated-time domain, where timings of impulses is instead fixed. Additionally, path constraints over the dense time horizon are reformulated as an equivalent set of isoperimetric constraints [25]. These two features improve performances of the optimization process: GTD allows to optimize both the location and timing of impulses; isoperimetric constraint reformulation ensures continuous-time constraint satisfaction without the need for

¹Ph.D. Student, William E. Boeing Department of Aeronautics and Astronautics, University of Washington, Seattle, WA 98195. fspada46@uw.edu

²Research Scientist, Mitsubishi Electric Research Laboratories (MERL), Cambridge, MA 02139. This work was not funded by MERL. elango@merl.com

³Professor, William E. Boeing Department of Aeronautics and Astronautics, University of Washington, Seattle, WA 98195. behcet@uw.edu

mesh-refinement, which is necessary for safety-critical applications [17], [18] but time-consuming. Especially in our application, nonlinear dynamics together with long planning horizons can quickly render mesh refinement approaches impractical for onboard, and potentially online, computations. The problem is then discretized using multiple shooting, exactly penalized using ℓ_1 penalty functions, and solved using *prox-linear* method [26], a convergence-guaranteed Sequential Convex Programming (SCP) algorithm. The contribution of this paper is twofold: firstly, for systems with jumps in the states, we prove equivalence between the satisfaction of a set of isoperimetric constraints and the satisfaction of path constraints over a continuous-time horizon; secondly, we test the outlined framework to solve a CROP, considering a target on a southern L_2 Near Rectilinear Halo Orbit (NRHO) along with KOZ and KIZ constraints. The location and timing of impulses are optimized to maximize residence time in the permitted region. Both a two-impulse strategy with initial coasting and a three-impulse strategy are implemented and tested.

Following the notation in this section, the OCP is outlined in section II. Time dilation and constraint augmentation are detailed in section III: for the former we show the transformation of the problem with free impulse timings into a problem where the impulse timings are fixed; for the latter we prove the equivalence between the satisfaction of path constraints over the continuous-time horizon and a set of isoperimetric constraints. The case study and corresponding numerical results are presented in sections IV-A, IV-B. Conclusions are finally drawn in section V.

A. Notation

\mathbb{R} , \mathbb{R}_+ , \mathbb{R}_{++} denote the full set, the nonnegative subset and the positive subset of real numbers. Vectors are denoted with boldface notation; $(\cdot)^E$ is such a matrix that $(\cdot)^E \mathbf{x} = (\cdot)$. $n_{(\cdot)}$ is the dimension of (\cdot) . Given $\mathcal{D} \subset \mathbb{R}$ defined as $\mathcal{D} := \bigcup_{i=1}^n \mathcal{D}_i$ and the continuous variable/function (\cdot) defined on \mathcal{D} , we indicate with $(\cdot)_i$ the restriction of (\cdot) to \mathcal{D}_i ; furthermore we denote with $(\cdot)_i^-$, $(\cdot)_i^+$ the values that $(\cdot)_i$ assumes respectively at the left and right endpoints of \mathcal{D}_i . Component-wise inequalities are indicated with the symbols \preceq , \succeq .

II. PROBLEM DEFINITION

Let us consider the time horizon $\mathcal{H} := [t_i, t_f]$, with fixed t_i and variable t_f . Let us divide \mathcal{H} into n_a arcs, indexed by the set \mathcal{I}^{n_a} , with $n_a + 1$ time instants, indexed by the set \mathcal{I}^{n_a+1} . The i^{th} arc \mathcal{H}_i is defined as $\mathcal{H}_i := [t_i, t_{i+1}]$, where endpoints are free; moreover, $t_i = t_1 < \dots < t_{n_a} < t_{n_a+1}$, where we replace t_f with t_{n_a+1} to avoid duplicate variables. An impulsive control $\Delta \mathbf{v}_i \in \mathbb{R}^{n_v}$ is applied at each t_i . The relative-to-target state of the chaser, the absolute state of the chaser and the absolute state of the target are respectively described by the state vector $\mathbf{x}_i \in \mathbb{R}^{n_x}$, the vector $\mathbf{X}_i \in \mathbb{R}^{n_x}$, $i \in \mathcal{I}^{n_a}$ and the assigned function $\mathbf{X}_T : \mathcal{H} \rightarrow \mathbb{R}^{n_x}$; therefore $\mathbf{x}_i := \mathbf{X}_i - \mathbf{X}_T(t)$.

The continuously differentiable function $\mathbf{f}^a : \mathbb{R}^{n_x} \times \mathcal{H} \rightarrow$

\mathbb{R}^{n_x} models the time-dependent absolute dynamics right-hand side (RHS). Given target initial state $\mathbf{X}_{T,i} \in \mathbb{R}^{n_x}$, the target state satisfies

$$\dot{\mathbf{X}}_T(t) = \mathbf{f}^a(\mathbf{X}_T(t), t), \quad t \in \mathcal{H}, \quad \mathbf{X}_T(t_i) = \mathbf{X}_{T,i} \quad (1)$$

Henceforth, we omit the dependency of states on t . The relative dynamics of the chaser with respect to target, indicated with $\mathbf{f} : \mathbb{R}^{n_x} \times \mathcal{H}_i \rightarrow \mathbb{R}^{n_x}$, reads

$$\mathbf{f}(\mathbf{x}_i, t) = \mathbf{f}^a(\mathbf{X}_T + \mathbf{x}_i, t) - \mathbf{f}^a(\mathbf{X}_T, t) \quad \left| \begin{array}{l} t \in \mathcal{H}_i, \\ \forall i \in \mathcal{I}^{n_a} \end{array} \right. \quad (2)$$

Dynamics are uncontrolled along each arc.

Chaser relative initial state is fixed to $\mathbf{x}_i \in \mathbb{R}^{n_x}$; introducing an additional variable vector, conveniently denoted as $\mathbf{x}_{n_a+1}^- \in \mathbb{R}^{n_x}$, the boundary conditions of the problem read

$$\begin{aligned} \mathbf{x}_1^- &= \mathbf{x}_1 + B \Delta \mathbf{v}_1 \\ \mathbf{x}_{i+1}^- &= \mathbf{x}_i^+ + B \Delta \mathbf{v}_{i+1} \quad i \in \mathcal{I}^{n_a} \end{aligned} \quad (3)$$

where the *allocation matrix* $B \in \mathbb{R}^{n_x \times n_v}$ allocates the components of $\Delta \mathbf{v}_i$ in the corresponding components of the state vector. A graphical representation of the presented framework is reported in Fig. 1.

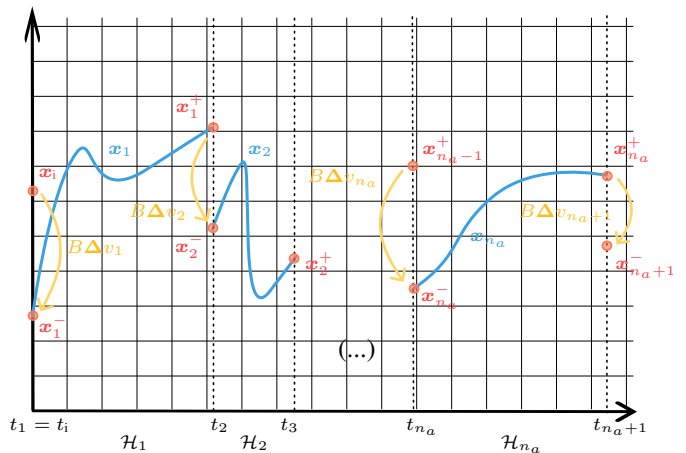


Fig. 1: One-dimensional representation of the relations between states and impulsive controls over the discretized time horizon.

Remark 1: While fixed final conditions are common in OCP formulations, we ignore them in this work. On one hand, the described framework still allows for imposing such conditions by constraining $\mathbf{x}_{n_a+1}^-$. On the other hand, the absence of fixed final conditions is addressed in this work through the chosen path constraints.

The continuously differentiable function $\mathbf{g} : \mathbb{R}^{n_x} \times \mathcal{H} \rightarrow \mathbb{R}^{n_g}$ and the function $\mathbf{G} : \mathbb{R}^{n_x} \times \mathbb{R}^{n_v} \rightarrow \mathbb{R}^{n_G}$ are the continuous-time and discrete-time inequality constraints functions; path constraints are respectively satisfied imposing $\mathbf{g}(\mathbf{x}_i, t) \preceq 0$, $t \in \mathcal{H}_i, \forall i \in \mathcal{I}^{n_a}$, and $\mathbf{G}(\mathbf{x}_i^-, \Delta \mathbf{v}_i) \preceq 0$, $\forall i \in \mathcal{I}^{n_a+1}$.

At last, the continuously differentiable functions $L : \mathbb{R}^{n_x} \times \mathbb{R}_+ \rightarrow \mathbb{R}$, $\mathcal{L} : \mathbb{R}^{n_v} \rightarrow \mathbb{R}$ make up for the terminal and discrete running costs.

By gathering the impulses in $\Delta \mathbf{V} \in \mathbb{R}^{n_v \times (n_a+1)}$, the subintervals bounds in $\mathbf{t} \in \mathbb{R}^{n_a+1}$ and the state trajectories and final state in $\chi \in \mathbb{R}^{n_x \times (n_a+1)}$, the final OCP reads

Problem 1 (P1)

$$\begin{aligned} & \underset{\chi, \mathbf{t}, \Delta \mathbf{V}}{\text{minimize}} && L(\mathbf{x}_{n_a+1}^-, t_{n_a+1}) + \sum_{i=1}^{n_a+1} \mathcal{L}(\Delta \mathbf{v}_i) \\ & \text{subject to} && \begin{cases} \dot{\mathbf{x}}_i = \mathbf{f}(\mathbf{x}_i, t) \\ \mathbf{g}(\mathbf{x}_i, t) \leq 0 \\ \mathbf{x}_{i+1}^- = \mathbf{x}_i^+ + B \Delta \mathbf{v}_{i+1} \\ \mathbf{G}(\mathbf{x}_i^-, \Delta \mathbf{v}_i) \leq 0 \\ \mathbf{x}_1^- = \mathbf{x}_1 + B \Delta \mathbf{v}_1 \\ t_1 = t_i \end{cases} \quad \forall i \in \mathcal{I}^{n_a} \end{aligned} \quad (4)$$

III. TIME DILATION, CONSTRAINT AUGMENTATION, AND SCP FRAMEWORK

Model of Problem 1 allows to optimize maneuvering times and includes continuous-time path constraints. Here, we describe two modifications to incorporate free-impulse time and path-constraints satisfaction within a single continuous-time fixed-impulse time problem. In Sec. III-A, we show how to cast the free-impulse time Problem 1 into a fixed-impulse time one; we then demonstrate in Sec. III-B the equivalence between the continuous-time satisfaction of the path constraints over \mathcal{H} and a set of isoperimetric constraints imposed on an additional state. In Sec. III-C we provide an overview of the discretization, ℓ_1 exact penalization and *prox-linear*, a convergence-guaranteed SCP method employed in the present work.

A. Generalized Time-Dilation

Define the continuously differentiable mapping $t : [0, n_a] \rightarrow \mathbb{R}_+$, and an additional continuous control input, the *dilation factor* $s : [0, n_a] \rightarrow \mathbb{R}_{++}$. Further definition of the *dilated time* $\tau \in [0, n_a]$ enables linking t, τ and s by the derivative map

$$s(\tau) = \frac{dt(\tau)}{d\tau} = t'(\tau) \quad (5)$$

where the notation $(\cdot)'$ denotes the derivative with respect to τ . t can be hence treated as an additional state. As before, we partition the dilated time horizon $\mathbf{H} := [0, n_a]$ into n_a arcs $\mathbf{H}_i := [\tau_i, \tau_{i+1}]$, $i \in \mathcal{I}^{n_a}$. Using chain-rule, dynamics are reformulated as

$$\begin{bmatrix} \mathbf{x}'_i \\ t'_i \end{bmatrix} = \begin{bmatrix} \dot{\mathbf{x}}_i \\ 1 \end{bmatrix} \frac{dt_i}{d\tau} = \begin{bmatrix} \dot{\mathbf{x}}_i \\ 1 \end{bmatrix} s_i, \quad \forall i \in \mathcal{I}^{n_a} \quad (6)$$

We finally fix the dilated times to the arbitrary values $\tau_i = i - 1$, $i \in \{1, \dots, n_a + 1\}$; this last passage allows to transform the original free-impulse time problem into a fixed-impulse time one; time dilation controls s_i , $i \in \mathcal{I}^{n_a}$, allow physical time to be maintained as an optimization variable. Therefore, Problem 1 is independent of the used time-domain representation.

B. Constraint reformulation

Consider the *exterior penalty functions* $q_{j,i} : \mathbb{R} \rightarrow \mathbb{R}_+$, $j = 1, \dots, n_g$, $i \in \mathcal{I}^{n_a}$, obeying the constraints

$$q_{j,i}(z) \begin{cases} = 0 & \text{if } z \leq 0 \\ > 0 & \text{otherwise} \end{cases} \quad (7)$$

and the *penalty functions* $\Lambda_i : \mathbb{R}^{n_x} \times \mathbf{H}_i \rightarrow \mathbb{R}_+$

$$\Lambda_i(\mathbf{x}_i, t_i) := \sum_{j=1}^{n_g} q_{j,i}(g_j(\mathbf{x}_i, t_i)) \quad (8)$$

where g_j denotes the scalar-valued elements of \mathbf{g} .

Remark 2: The functions $q_{j,i}$ and, consequently, Λ_i , can generally be selected based on the considered interval \mathbf{H}_i . While we assume fixed q_j and Λ valid $\forall i \in \mathcal{I}^{n_a}$, one could choose different exterior penalty functions: for example, this can prioritize satisfaction of constraints in one interval over another. Importantly, the choice of different penalty functions does not affect the subsequent discussion.

Given the continuity of \mathbf{g} and s , and for \mathbf{x}_i, t_i evolving according to Eq. (6) over $\mathbf{H}_i \forall i \in \mathcal{I}^{n_a}$, the mapping $\tau \in \mathbf{H}_i \mapsto s_i(\tau) \Lambda(\mathbf{x}_i(\tau), t_i(\tau))$ is continuous. In addition, Λ and s are respectively nonnegative and positive. As a consequence, the direct implication of the following holds

$$\int_{\tau_i}^{\tau_{i+1}} s_i(\tau) \Lambda(\mathbf{x}_i(\tau), t_i(\tau)) d\tau = 0, \quad \forall i \in \mathcal{I}^{n_a} \quad (9)$$

$$\Leftrightarrow \Lambda(\mathbf{x}_i(\tau), t_i(\tau)) = 0, \quad \tau \in \mathbf{H}_i, \forall i \in \mathcal{I}^{n_a}$$

The inverse implication (the 'upwards' one) can be verified by direct proof easily. In virtue of definitions in Eqs. (7), (8), the second condition in Eq. (9) is equivalent to $\mathbf{g}(\mathbf{x}_i(\tau), t_i(\tau)) \leq 0$, $\tau \in \mathbf{H}_i$. Therefore, the first condition in Eq. (9) is verified $\forall i \in \mathcal{I}^{n_a}$, *i.e.* a set of *isoperimetric constraints*, if and only if path constraints are satisfied for $\tau \in [\tau_i, \tau_{i+1}]$, $\forall i \in \mathcal{I}^{n_a}$.

As a next step, consider the additional state $y \in \mathbb{R}$ and the two-point boundary value problems (TPBVPs)

$$\begin{cases} y'_i(\tau) = s_i(\tau) \Lambda(\mathbf{x}_i(\tau), t_i(\tau)), & \tau \in \mathbf{H}_i \\ y_i(\tau_i) = y_i(\tau_{i+1}) \end{cases} \Bigg|_{i \in \mathcal{I}^{n_a}} \quad (10)$$

y_i satisfies Eq. (10) $\forall i \in \mathcal{I}^{n_a}$ if and only if the set of isoperimetric constraints from Eq. (9) is satisfied.

Let us reason over the generic interval \mathbf{H}_i . $s_i(\tau) \Lambda(\mathbf{x}_i(\tau), t_i(\tau))$ is continuous, hence Riemann-integrable; a scalar Initial Value Problem (IVP) with assigned initial condition $y_i(\tau_i)$ and derivative $s_i(\tau) \Lambda(\mathbf{x}_i(\tau), t_i(\tau))$ is solved, then, by

$$y_i(\tau_{i+1}) = y_i(\tau_i) + \int_{\tau_i}^{\tau_{i+1}} s_i(\tau) \Lambda(\mathbf{x}_i(\tau), t_i(\tau)) d\tau \quad (11)$$

From the previous, it is straightforward to see that a trajectory solving the TPBVP in Eq. (10) satisfies the isoperimetric constraint in Eq. (9); the converse is as well steadily verified. For simplicity, we can fix $y_1(\tau_1) = 0$; thus boundary conditions for all TPBVPs are as well fixed.

Summing up, we have proved that satisfaction of continuous-time path constraints ensures existence of an augmented scalar state $y \in \mathbb{R}$, solving the TPBVPs in Eq. (10), and vice versa.

Remark 3: In this formulation equality path constraints and continuous external control have been ignored in each \mathbf{H}_i . However, the equality path constraints can be incorporated into the penalty function Λ with appropriate additional exterior penalty functions; the described proofs remain valid under mild regularity assumptions on controls and equality constraints [25].

Remark 4: As a gradient-based optimization algorithm will be used, it is of stark importance to pick continuously differentiable exterior penalty functions, e.g.

$$\begin{aligned} q_j(z) &= \max\{0, z\}^n \\ \Lambda(\mathbf{x}_i, t_i) &= \sum_{j=1}^{n_g} \max\{0, g_j(\mathbf{x}_i, t_i)\}^n, \quad n > 1 \end{aligned} \quad (12)$$

At this stage, it is possible to finalize reformulation of Problem 1. Let us consider the augmented state $\tilde{\mathbf{x}}_i \in \mathbb{R}^{n_x+2}$, defined over \mathbf{H}_i as

$$\tilde{\mathbf{x}}_i = [\mathbf{x}_i^T, y_i, t_i]^T \quad (13)$$

Similarly as what done before, from use of chain-rule it results

$$\tilde{\mathbf{x}}'_i = \begin{bmatrix} \mathbf{f}(\mathbf{x}_i, t_i) \\ \Lambda(\mathbf{x}_i, t_i) \\ 1 \end{bmatrix} s_i := \mathbf{F}(\tilde{\mathbf{x}}_i, s_i) \quad \forall i \in \mathcal{I}^{n_a} \quad (14)$$

Let us gather the dilation factors into $\mathbf{s} := [s_1, s_2, \dots, s_{n_a}]^T$, the initial conditions $\mathbf{x}_i, y_i := 0$ and t_i into the initial condition $\tilde{\mathbf{x}}_i = [\mathbf{x}_i^T, y_i, t_i]^T$. Furthermore, let $\tilde{\mathbf{B}} \in \mathbb{R}^{(n_x+2) \times n_v}$ define the augmented allocation matrix, $\tilde{\boldsymbol{\chi}} \in \mathbb{R}^{(n_x+2) \times (n_a+1)}$ gather the augmented state trajectories and augmented final state and $\tilde{\mathbf{L}}: \mathbb{R}^{n_x+2} \rightarrow \mathbb{R}$ generalize L according to $\tilde{L}(\tilde{\mathbf{x}}) := L({}^x E \tilde{\mathbf{x}}, {}^t E \tilde{\mathbf{x}})$. The original OCP gets then rearranged as

Problem 2 (P2)

$$\begin{aligned} &\text{minimize}_{\boldsymbol{\chi}, \mathbf{t}, \Delta \mathbf{V}} \quad \tilde{L}(\tilde{\mathbf{x}}_{n_a+1}^-) + \sum_{i=1}^{n_a+1} \mathcal{L}(\Delta \mathbf{v}_i) \\ &\text{subject to} \quad \left. \begin{aligned} &\tilde{\mathbf{x}}'_i = \mathbf{F}(\tilde{\mathbf{x}}_i, s_i) \\ &s_i > 0 \\ &{}^y E(\tilde{\mathbf{x}}_{i+1} - \tilde{\mathbf{x}}_i) = 0 \end{aligned} \right| \forall i \in \mathcal{I}^{n_a} \\ &\quad \left. \begin{aligned} &\tilde{\mathbf{x}}_{i+1}^- = \tilde{\mathbf{x}}_i^+ + \tilde{\mathbf{B}} \Delta \mathbf{v}_{i+1} \quad \forall i \in \mathcal{I}^{n_a} \\ &\mathbf{G}({}^x E \tilde{\mathbf{x}}_i^-, \Delta \mathbf{v}_i) \preceq 0 \quad \forall i \in \mathcal{I}^{n_a+1} \\ &\tilde{\mathbf{x}}_1^- = \tilde{\mathbf{x}}_1 + \tilde{\mathbf{B}} \Delta \mathbf{v}_1 \end{aligned} \right| \end{aligned} \quad (15)$$

C. Discretization, penalization and SCP

Parameterization and discretization transform the problem in a finite-dimensional one. As first step, we *parameterize* the controls s_i : we approximate each function s_i as a linear combination of n_S basis functions $\Gamma_{j,i}: \mathbf{H}_i \rightarrow \mathbb{R}, j = 1, \dots, n_S$ of coefficients $\mathbf{S}_i \in \mathbb{R}^{n_S}$. By choosing $\Gamma_{j,i}, \Gamma_{j,i+1}$

that differ only for a domain translation of $\tau_{i+1} - \tau_i$, the dependency on i drops and it results

$$\begin{aligned} \nu(\mathbf{S}_i, \tau) &:= [\Gamma_1(\tau), \dots, \Gamma_{n_S}(\tau)] \mathbf{S}_i \\ s_i(\tau) &= \nu(\mathbf{S}_i, \tau) \end{aligned} \quad \left| \begin{array}{l} \tau \in \mathbf{H}_i \\ \forall i \in \mathcal{I}^{n_a} \end{array} \right. \quad (16)$$

Followingly, we *discretize* each arc into K subarcs of equal length with $K+1$ nodes; subarcs and nodes are respectively indexed by \mathcal{I}^K and \mathcal{I}^{K+1} . We replace each variable $\tilde{\mathbf{x}}_i$ with $K+1$ augmented state variables $\tilde{\mathbf{x}}_i^k, k \in \mathcal{I}^{K+1}$; then we enforce dynamical feasibility via *multiple-shooting*, i.e. by integrating dynamics on time. Defining $\tau_i^k := \tau_i + (k-1)/K$, the following constraints are added

$$\begin{aligned} \tilde{\mathbf{x}}_i^1 &= \tilde{\mathbf{x}}_i^- \\ \tilde{\mathbf{x}}_i^{k+1} &= \tilde{\mathbf{x}}_i^k + \int_{\tau_i^k}^{\tau_i^{k+1}} \mathbf{F}(\tilde{\mathbf{x}}_i^k, \nu(\mathbf{S}_i, \tau)) d\tau \quad \forall k \in \mathcal{I}^K \\ \tilde{\mathbf{x}}_i^{K+1} &= \tilde{\mathbf{x}}_i^+ \end{aligned} \quad (17)$$

Introducing the mapping

$$\begin{aligned} \mathbf{F}_{i,k} &: (\tilde{\mathbf{x}}_i^k, \tilde{\mathbf{x}}_i^{k+1}, \mathbf{S}_i) \mapsto \\ &\mapsto \tilde{\mathbf{x}}_i^{k+1} - \tilde{\mathbf{x}}_i^k - \int_{\tau_i^{k-1}}^{\tau_i^k} \mathbf{F}(\tilde{\mathbf{x}}_i^k, \nu(\mathbf{S}_i, \tau)) d\tau \end{aligned} \quad (18)$$

dynamical feasibility can be imposed as $\mathbf{F}_{i,k} = 0, \forall i \in \mathcal{I}^{n_a}, \forall k \in \mathcal{I}^K$. Discretization of the boundary conditions on y leads instead to ${}^y E(\tilde{\mathbf{x}}_i^{k+1} - \tilde{\mathbf{x}}_i^k) = 0, \forall i \in \mathcal{I}^{n_a}, \forall k \in \mathcal{I}^K$.

Remark 5: Gradients of the discretized boundary conditions and discretized shooting constraints for y with respect to y_i^k are, for feasible trajectories, parallel [25]. This feature violates Linear Independence Constraint Qualification, a typical requirement ensuring reliability of a solution obtained with numerical optimization algorithms [27]. As a consequence, we avoid this pathological scenario by relaxing the boundary conditions on y as

$${}^y E(\tilde{\mathbf{x}}_i^{k+1} - \tilde{\mathbf{x}}_i^k) < \varepsilon, \quad \forall i \in \mathcal{I}^{n_a}, \forall k \in \mathcal{I}^K$$

given a small scalar value ε . As shown later in the results, this relaxation does not negatively affect the quality of the constraint satisfaction.

The remaining constraints retain the same form as in Problem 2.

Remark 6: Whilst sensitivity to coarse initial guesses is mitigated by use of multiple-shooting, such last technique adds variables to the solution process; thus increasing computational times. For this reason, *single-shooting* is sufficient and beneficial when sensitivity issues are not encountered.

We then proceed by *exactly penalizing* the nonconvex constraints, i.e. we incorporate them in the objective function using an ℓ_1 penalization. Let us gather the augmented state trajectories $\tilde{\mathbf{x}}_i^k, i \in \mathcal{I}^{n_a}, k \in \mathcal{I}^{K+1}$, the parameterized controls $\mathbf{S}_i, i \in \mathcal{I}^{n_a}$ and the impulsive controls $\Delta \mathbf{v}_i, i \in \mathcal{I}^{n_a+1}$ in the single vector \mathbf{z} ; moreover, let the set \mathcal{Z} contain the augmented states and dilation factors feasible with respect to the convex constraints of the discretized problem, and let $\tilde{\mathcal{L}}_{\mathcal{Z}}$

be its indicator function. We introduce the objective function $\Theta_\gamma : \mathbb{R}^{n_z} \rightarrow \mathbb{R}$ and define it as

$$\begin{aligned} \Theta_\gamma(\mathbf{z}) := & \tilde{L}(\tilde{\mathbf{x}}_{n_a+1}^-) + \sum_{i=1}^{n_a+1} \mathcal{L}(\Delta \mathbf{v}_i) + \tilde{\mathcal{I}}_{\mathcal{Z}}(\mathbf{z}) + \\ & + \gamma \sum_{i=1}^{n_a+1} \max\{0, \mathbf{G}({}^x E \tilde{\mathbf{x}}_i^-, \Delta \mathbf{v}_i)\} + \\ & + \gamma \sum_{i=1}^{n_a+1} \sum_{k=1}^{K+1} \|\mathbf{F}_{i,k}(\tilde{\mathbf{x}}_i^k, \tilde{\mathbf{x}}_i^{k+1}, \mathbf{S}_i)\|_1 \end{aligned} \quad (19)$$

where $\gamma \in \mathbb{R}_+$ is a large finite value. We have exactly penalized the violation of nonconvex constraints by means of nonsmooth penalty functions, as the ℓ_1 -norm. Therefore, for a finite high value of γ , the solution of the following unconstrained problem

$$\text{Problem 3 (P3)} \quad \underset{\mathbf{z}}{\text{minimize}} \quad \Theta_\gamma(\mathbf{z}) \quad (20)$$

satisfies the Karush–Kuhn–Tucker (KKT) conditions of the original constrained problem and is a strict local minimizer of it [27]. No approximation has been introduced up to here, except for the relaxation of the boundary conditions on y . This means that, solving Problem 3, we can retrieve the exact solution of Problem 1.

Problem 3, however, is still nonlinear. We therefore use *prox-linear* method, an SCP algorithm that minimizes convex-composite functions with guaranteed convergence. More specifically, prox-linear treats objective functions of type $\Theta_\gamma(\mathbf{z}) = J(\mathbf{z}) + H(\mathbf{c}(\mathbf{z}))$, where J is a proper closed convex function, H is an α -Lipschitz continuous convex function and \mathbf{c} is a potentially nonconvex and continuously differentiable function with β -Lipschitz continuous gradient. With respect to our formulation, J corresponds to the indicator function $\tilde{\mathcal{I}}_{\mathcal{Z}}$; \mathbf{c} gathers a) the objective function, b) the discrete path constraints and c) the shooting constraints. Finally, H components are a) the identity function, for the objective function, b) the function $\max\{0, (\cdot)\}$, for the discrete path constraints and c) the ℓ_1 -norm, for each shooting constraint.

Given the current iterate \mathbf{z}_j , prox-linear minimizes iteratively the following convex approximation of Θ_γ

$$\begin{aligned} \Theta_\gamma^\rho(\mathbf{z}, \mathbf{z}_j) = & J(\mathbf{z}) + H(\mathbf{c}(\mathbf{z}_j)) + \\ & + \nabla \mathbf{c}(\mathbf{z}_j)(\mathbf{z} - \mathbf{z}_j) + \frac{1}{2\rho} \|\mathbf{z} - \mathbf{z}_j\|_2 \end{aligned} \quad (21)$$

where $\rho \in \mathbb{R}_+$ is a tuning parameter that influences the proximal term weight. Defining the *prox-gradient mapping* as $\mathcal{G}_\rho : \mathbf{z} \mapsto \mathbb{R}$ as

$$\mathcal{G}_\rho(\mathbf{z}) := \frac{1}{\rho} \left(\mathbf{z} - \underset{\tilde{\mathbf{z}}}{\operatorname{argmin}} \Theta_\gamma^\rho(\tilde{\mathbf{z}}, \mathbf{z}_j) \right) \quad (22)$$

the following condition is verified at each iteration of the algorithm [26]

$$\Theta_\gamma(\mathbf{z}_{j+1}) \leq \Theta_\gamma(\mathbf{z}_j) + \left(\alpha\beta - \frac{1}{\rho} \right) \|\rho \mathcal{G}_\rho(\mathbf{z}_j)\|^2, \quad (23)$$

Therefore, the condition $\rho \leq 1/(\alpha\beta)$ is sufficient to ensure that the objective function decreases monotonically. At last, consider the initial guess \mathbf{z}_1 , a lower bound Θ_γ^* for Θ_γ and a stopping tolerance ϵ . If $\rho \leq 1/(\alpha\beta)$, the number of iterations required to bring $\|\mathcal{G}_\rho\|^2$ within some tolerance ϵ is bounded. More specifically,

$$j \geq \frac{2\alpha\beta(\Theta_\gamma(\mathbf{z}_1) - \Theta_\gamma^*)}{\epsilon} \Rightarrow \|\mathcal{G}_\rho(\mathbf{z}_j)\|^2 < \epsilon \quad (24)$$

In practical applications, a maximum number of iterations j_{\max} is added to prox-linear for contingency scenarios. Algorithm 1 synthesizes steps of prox-linear.

A local minimum \mathbf{z}^* computed with prox-linear is close to a point where first-order optimality of $\Theta_\gamma(\mathbf{z})$ is small [26]. This point in turn, for high finite γ , is close to a strict local minimizer of Problem 1.

Remark 7: γ and ρ are tuning parameters and, as such, choosing them properly is crucial to ensure algorithm convergence. γ is heuristically selected to grant satisfactory results; backtracking schemes are employed to update ρ [26] and grant successful convergence to a local minimum.

Algorithm 1 Prox-linear Method

Require: j_{\max}, ϵ, ρ

Initialize: \mathbf{z}_1

$j \leftarrow 1$

while $j \leq j_{\max}$ **and** $\|\mathcal{G}_\rho(\mathbf{z}_j)\| > \epsilon$ **do**

$\mathbf{z}_{j+1} \leftarrow \underset{\mathbf{z}}{\operatorname{argmin}} \Theta_\gamma^\rho(\mathbf{z}, \mathbf{z}_j)$

$j \leftarrow j + 1$

end while

Ensure: \mathbf{z}_j

IV. NUMERICAL EXAMPLE

A. Problem definition

We assume a target on a 9:2 resonant southern NRHO emanating from L_2 in the Circular Restricted 3 Body (CR3B) model. Motion of each spacecraft is described in the Earth-Moon synodic reference frame; the absolute dynamics RHS, normalized with respect to mean Earth-Moon distance and angular speed ω , reads

$$\mathbf{f}^a = \begin{bmatrix} \mathbf{V} \\ R_x + 2V_y - (1 - \mu) \frac{R_{1,x}}{R_1^3} - \mu \frac{R_{2,x}}{R_2^3} \\ R_y - 2V_x - (1 - \mu) \frac{R_{1,y}}{R_1^3} - \mu \frac{R_{2,y}}{R_2^3} \\ -(1 - \mu) \frac{R_{1,z}}{R_1^3} - \mu \frac{R_{2,z}}{R_2^3} \end{bmatrix} \quad (25)$$

where \mathbf{R}_1 and \mathbf{R}_2 are the vectorial relative distances from Earth and Moon, and R_1 and R_2 their norms. Fig. 2 shows the target and the chaser in the synodic Earth-Moon reference frame.

Initial state of the target is fixed at perilune: the function $\mathbf{X}_T(t)$ that describes the target state likewise parameterizes in time the NRHO on which the target resides. The chaser

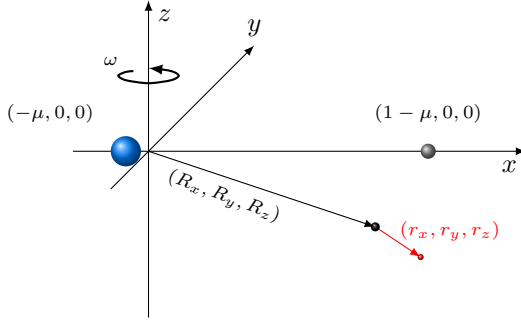


Fig. 2: Earth, Moon, target and chaser spacecrafts (in black and red) in the normalized Earth-Moon synodic reference frame.

can fire n_a impulses, each of maximum magnitude Δv_{\max} . In addition, the target must remain inside a sphere of radius r_{\max} and outside a sphere of radius r_{\min} . Both spheres are centered at the target. The objective is maximizing the residence time of the chaser in the admissible region, given the available control actuation capability. Problem is hence formulated as

Problem 4 (P4)

$$\begin{aligned}
 & \underset{\chi, t, \Delta V}{\text{minimize}} && -t_{n_a+1} \\
 & \text{subject to} && \begin{cases} \dot{\mathbf{x}}_i = \mathbf{f}(\mathbf{x}_i, t) \\ \|{}^r E \mathbf{x}_i\|_2 - r_{\max} \leq 0 \\ r_{\min} - \|{}^r E \mathbf{x}_i\|_2 \leq 0 \end{cases} && \begin{cases} t \in \mathcal{H}_i \\ \forall i \in \mathcal{I}^{n_a} \end{cases} \\
 & && \begin{cases} \mathbf{x}_{i+1}^- = \mathbf{x}_i^+ + B \Delta \mathbf{v}_{i+1} \\ \|\Delta \mathbf{v}_i\|_2 \leq \Delta v_{\max} \\ \mathbf{x}_1^- = \mathbf{x}_1 + B \Delta \mathbf{v}_1 \\ t_1 = 0 \end{cases} && \begin{cases} \forall i \in \mathcal{I}^{n_a} \\ \forall i \in \mathcal{I}^{n_a+1} \end{cases}
 \end{aligned} \quad (26)$$

B. Numerical results

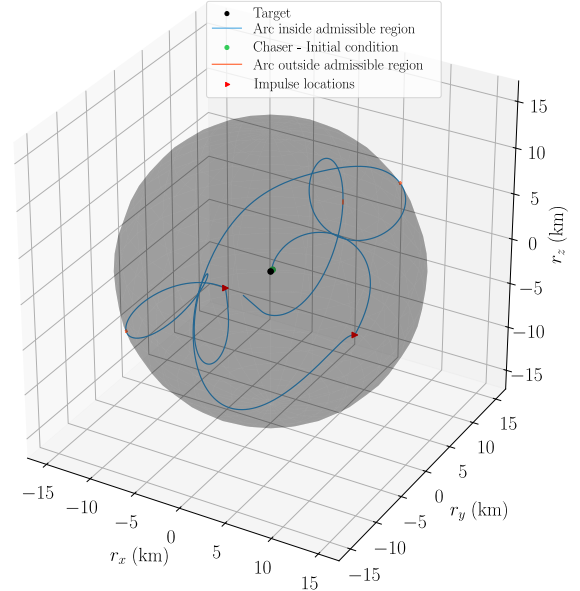
A two and a three-impulse strategy are tested. The devised two-impulse strategy consists of an initial free-drift arc, followed by two impulses; the three-impulse strategy allows an initial impulse as well. In both cases, an initial position deviation of 400 m is accounted for; for the two-impulse strategy, deviation is along the y axis, for the two-impulse strategy, it is along the x axis. Common problem parameters are reported in Tab. I. In both cases, a First-Order Hold parameterization for the dilation factor has been used.

TABLE I: Data for the two scenarios

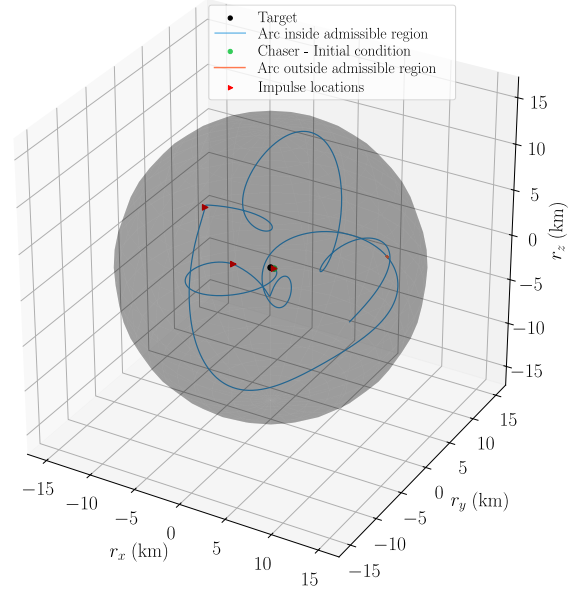
Physical quantity	Value	Unit
$R_T(0)^\dagger$	[0.987360158, 0, 0.008773055]	(-)
$V_T(0)$	[0, 1.634461555, 0]	(-)
r_{\max}	15	km
r_{\min}	0.3	km
Δv_{\max}	$2.5 \cdot 10^{-4}$	km/s

[†] For conversion purposes, Earth-Moon mean distance is approximated to 384400 km

By letting the system drift from its initial conditions without control for one full period (6 days and a half), distance-to-target peaks at approximately 200 km for the 3-impulse case, and at 50 km for the two-impulse case; this has been verified during simulations, and is not reported for space limitations. The need for control is then evident. The final trajectories are represented in Fig. 3 for both strategies; small arcs of KIZ constraint violation appear in both cases; except for these, the trajectories lie completely within the admissible zone.



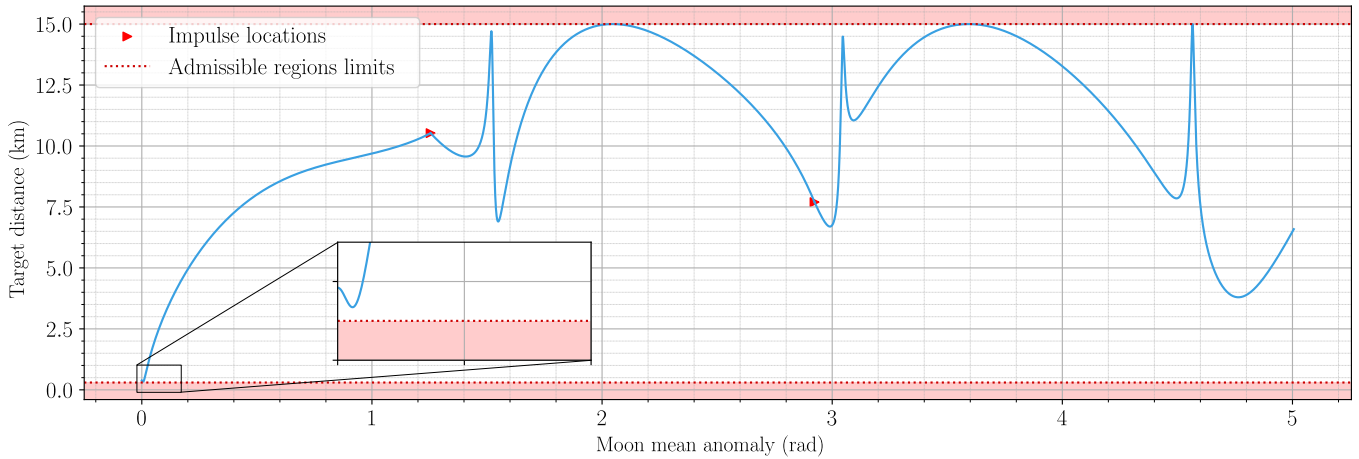
(a) Coasting and 2-impulse strategy



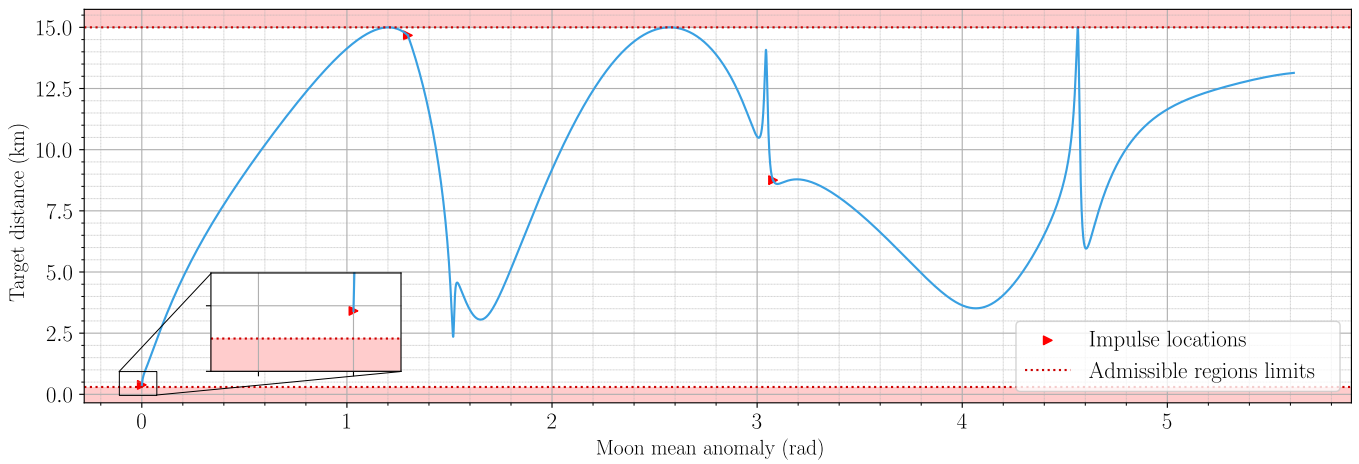
(b) 3-impulse strategy

Fig. 3: Relative trajectories in the synodic reference frame

Table II formalizes the results for the two case studies. In both cases the proposed predictive framework grants at least 22 days of bounded loitering. A single segment for each arc



(a) Coasting and 2-impulse strategy



(b) 3-impulse strategy

Fig. 4: Relative-to-target distance, with nonadmissible zones and zoom-ins on the initial hours of flight

TABLE II: Merit parameters for the two scenarios

Parameter	Value	
	2-impulses	3-impulses
$t_{n_{a+1}}$	22.3 d	25.0 d
Δv_1	(-)	19.5 cm/s
Δv_2	7.8 cm/s	5.2 cm/s
Δv_3	7.4 cm/s	4.9 cm/s
CPU time [†] /it.	6.34 ms	5.46 ms
its.	71	55
CPU time	454 ms	301 ms

[†] Tests have been run on Julia 1.10.3, on a MacBook 2023 with Apple M3 Pro, 18GB of unified memory. Mosek has been used as convex solver.

is used in the discretization step: CPU times per iteration are extremely contained; literature results demonstrate that such factor can further drop by a factor of 2 when a custom solver is used. The discretization time associated with integration of a single subproblem penalizes the full algorithm; such time is approximately two orders of magnitude higher than the CPU time required to solve the subproblem itself. On the other

hand, this limitation is common to shooting techniques and is not due to the proposed state augmentation; computing the RHS for the variables y and t is not penalizing. Furthermore, dedicated integrators, which were not the focus of this work, can solve this problem. In addition, the proposed predictive control strategy ensures that a single node is sufficient to capture the full amount of violations of the path constraints, no matter the duration of the coasting arc; as shown in Fig. 4, indeed, the distance relative to target remains within the acceptable region for both case studies. Notably, GTD influence is evident by comparing the length of the first and of the last arcs. Whilst the guess provided to the algorithm considers nodes at equally spaced times, the third arc is approximately the double of the first at convergence. This confirms the performance increment provided by GTD. The partial constraint violation highlighted in Fig. 3 falls within the bounds related with the relaxation in Sec. III-C; constraint violation that can be quantified and contained. More importantly, no violation of the KOZ constraint is verified at all, as highlighted by the zoom-ins in Fig. 4. The proposed technique exploits shooting with a single node for

each cost arc whilst ensuring constraint satisfaction over the continuous-time horizon. Mesh-refinement techniques constitute state-of-the-art for direct optimization and try to ensure constraint satisfaction over the continuous time-horizon by adding nodes at each iteration of the direct optimization; this number of nodes may be prohibitively high. The aspect is evident from Fig. 4a, where the last 'touch' of the keep-in zone bound occurs when the rate of change for the relative distance is high: refining trajectory sections with such strong time gradients would require adding significantly more variables, thus impacting on computational times negatively.

V. CONCLUSIONS

In this work, we have proposed and tested a strategy to compute relative constrained trajectories with impulsive controls. We have optimized location and timing of impulses; with few nodes, our approach has successfully satisfied path constraints throughout the entire computed time horizon. The framework has been tailored for a specific application in the double Earth-Moon gravitational regime. A Sequential Convex Programming algorithm has been used, showing fast solution computation and adaptability to different scenarios.

REFERENCES

- [1] K. Yamanaka and F. Ankersen, "New state transition matrix for relative motion on an arbitrary elliptical orbit," *Journal of Guidance, Control, and Dynamics*, vol. 25, no. 1, pp. 60–66, Jan. 2002.
- [2] H. Yan, S. R. Vadali, and K. T. Alfriend, "State Transition Matrix for Relative Motion Including J2 and Third-Body Perturbations," Univelt, 2014.
- [3] G. Franzini and M. Innocenti, "Relative Motion Dynamics in the Restricted Three-Body Problem," *Journal of Spacecraft and Rockets*, vol. 56, no. 5, pp. 1322–1337, Sep. 2019.
- [4] National Aeronautics and Space Administration, *ISS Safety Requirements Document*, International Space Station Program, Sep. 2019.
- [5] J. L. Goodman, "History of space shuttle rendezvous and proximity operations," *Journal of spacecraft and rockets*, vol. 43, no. 5, pp. 944–959, Sep. 2006.
- [6] S. B. Broschart and D. J. Scheeres, "Control of Hovering Spacecraft Near Small Bodies: Application to Asteroid 25143 Itokawa," *Journal of Guidance, Control, and Dynamics*, vol. 28, no. 2, pp. 343–354, Mar. 2005.
- [7] V. Martinusi and P. Gurfil, "Analytical Derivation of Single-Impulse Maneuvers Guaranteeing Bounded Relative Motion Under J2," *Journal of Guidance, Control, and Dynamics*, vol. 37, no. 1, pp. 233–242, Nov. 2014.
- [8] Y. He, R. Armellin, and M. Xu, "Bounded relative orbits in the zonal problem via high-order Poincaré maps," *Journal of Guidance, Control, and Dynamics*, vol. 42, no. 1, pp. 91–108, Jan. 2019.
- [9] Z. Dang, Z. Pan, H. Zhou, and H. Zhang, "Bounded relative motions near Keplerian orbits in spherical coordinates," *Advances in Space Research*, vol. 66, no. 11, pp. 2654–2666, Dec. 2020.
- [10] M. Dominguez and K. C. Howell, "Preliminary Design Strategy for Long-Term Loitering Orbits in Cislunar Space," in *AAS/AIAA Astrodynamics Specialist Conference 2024*, vol. 175.
- [11] F. Khoury and K. C. Howell, "Orbital rendezvous and Spacecraft Loitering in the Earth-Moon System," in *AAS/AIAA Astrodynamics Specialist Conference 2020*, vol. 175, Univelt.
- [12] C. Sandel and R. Sood, "Natural and forced spacecraft loitering in a near rectilinear halo orbit," *Journal of Astronautical Sciences*, vol. 71, no. 3, Jun. 2024.
- [13] S. B. Broschart and D. J. Scheeres, "Boundedness of spacecraft hovering under dead-band control in time-invariant systems," *Journal of Guidance, Control, and Dynamics*, vol. 30, no. 2, pp. 601–610, Mar. 2007.
- [14] P. R. Arantes Gilz, M. Joldes, C. Louembet, and F. Camps, "Stable model predictive strategy for rendezvous hovering phases allowing for control saturation," *Journal of Guidance, Control, and Dynamics*, vol. 42, no. 8, pp. 1658–1675, Aug. 2019.
- [15] J. C. Sanchez, C. Louembet, F. Gavilan, and R. Vazquez, "Event-based impulsive control for spacecraft rendezvous hovering phases," *Journal of Guidance, Control, and Dynamics*, vol. 44, no. 10, pp. 1794–1810, Oct. 2021.
- [16] C. Petersen, R. J. Caverly, S. Phillips, and A. Weiss, "Safe and constrained rendezvous, proximity operations, and docking," in *2023 American Control Conference (ACC)*, vol. 73, IEEE, May 2023, pp. 3645–3661.
- [17] A. Richards, T. Schouwenaars, J. P. How, and E. Feron, "Spacecraft planning with avoidance constraints using mixed-integer linear programming," *Journal of Guidance, Control, and Dynamics*, vol. 25, no. 4, pp. 755–764, Jul. 2002.
- [18] C. Ranieri, "Path-constrained trajectory optimization for proximity operations," in *AIAA/AAS Astrodynamics Specialist Conference and Exhibit*, Reston, Virginia: American Institute of Aeronautics and Astronautics, Aug. 2008.
- [19] Q. Li, S. Song, C. Sun, Q. Gou, and Z. Niu, "Robust output-feedback control for spacecraft proximity operations with forbidden zone," *IEEE Transactions on Aerospace and Electronic Systems*, vol. 58, no. 1, pp. 96–107, Feb. 2022.
- [20] A. Weiss, M. Baldwin, R. S. Erwin, and I. Kolmanovsky, "Model predictive control for spacecraft rendezvous and docking: Strategies for handling constraints and case studies," *IEEE transactions on control systems technology: a publication of the IEEE Control Systems Society*, vol. 23, no. 4, pp. 1638–1647, Jul. 2015.
- [21] C. Zagaris, H. Park, J. Virgili-Llop, R. Zappulla II, M. Romano, and I. Kolmanovsky, "Model predictive control of spacecraft relative motion with convexified keep-out-zone constraints," *Journal of Guidance, Control, and Dynamics*, pp. 1–9, Jun. 2018.
- [22] J. C. Sanchez, F. Gavilan, and R. Vazquez, "Chance-constrained Model Predictive Control for Near Rectilinear Halo Orbit spacecraft rendezvous," *Aerospace science and technology*, vol. 100, no. 105827, p. 105 827, May 2020.
- [23] D. Aguilar-Marsillach, S. D. Cairano, and A. Weiss, "Abort-safe spacecraft rendezvous on elliptic orbits," *IEEE transactions on control systems technology: a publication of the IEEE Control Systems Society*, pp. 1–16, 2022.
- [24] A. G. Kamath, P. Elango, Y. Yu, *et al.*, "Real-time sequential conic optimization for multi-phase rocket landing guidance," *IFAC-PapersOnLine*, vol. 56, no. 2, pp. 3118–3125, 2023.
- [25] P. Elango, D. Luo, A. G. Kamath, S. Uzun, T. Kim, and B. Açıkmeşe, "Successive convexification for trajectory optimization with continuous-time constraint satisfaction," *arXiv [math.OC]*, Apr. 2024.
- [26] D. Drusvyatskiy and A. S. Lewis, "Error bounds, quadratic growth, and linear convergence of proximal methods," *Mathematics of operations research*, vol. 43, no. 3, pp. 919–948, Aug. 2018.
- [27] J. Nocedal and S. Wright, *Numerical optimization*, en. Springer Science & Business Media, Dec. 2006.